Acta Materialia 99 (2015) 130–139

Contents lists available at ScienceDirect

Acta Materialia

journal homepage: www.elsevier.com/locate/actamat

Dislocation multiplication mechanisms – Glissile junctions and their role on the plastic deformation at the microscale

Markus Stricker *, Daniel Weygand [1]

Institute for Applied Materials, Karlsruhe Institute of Technology, Engelbert-Arnold-Straße 4, 76131 Karlsruhe, Germany

ARTICLE INFO

Article history:
Received 30 March 2015
Revised 29 July 2015
Accepted 30 July 2015
Available online 8 August 2015

Keywords:
Discrete dislocation dynamics
Dislocation multiplication
Glissile junction

ABSTRACT

Dislocation junctions are considered to control the hardening behavior of crystalline materials during plastic deformation. Here the influence of the glissile junction on the plastic deformation of microscale samples is investigated, based on discrete dislocation dynamics simulation results. It is found that with increasing dislocation density ρ, sample size d, which can be collapsed into a single dimensionless parameter $d\sqrt{\rho}$, and an increasing number of activated slip systems due to different global crystallographic orientations, the glissile junction forms frequently and can bow out easily, acting as an effective source. The resulting new dislocations are mobile and contribute to the macroscopic plastic deformation on the order of 30–60%. In the size regime from 0.5 to 2 μm and dislocation densities in the range of 10^{12}–10^{14} m^{-2}, the glissile junction is therefore an important source for generating mobile dislocation density. Furthermore a significant correlation between stress drops and activity of dislocations originating from glissile junctions is found. A rate formulation is proposed to include these findings in crystal plasticity or continuum dislocation density frameworks.

1. Introduction

Plasticity is caused by the motion of dislocations through the crystalline lattice. Junctions of dislocations during the plastic flow play a key role in the macroscopic deformation behavior, e.g. hardening is considered to be due to junctions of dislocations gliding on different slip systems [1–3]. But not all junctions necessarily lead to hardening. In face centered cubic (fcc) crystals, four types of junctions are possible: the Lomer, Hirth, collinear junctions and the glissile junction [4]. While the first three form locks which locally block the further glide motion of dislocations and act as a barrier to other dislocations of the slip systems involved [5], the glissile junction is able to produce new dislocation density, mobile on a new slip system. A recent work [6] shows that the overall contribution to the plastic deformation, which can be attributed to glissile junctions and their products, often reaches values of 20% or more and a fraction of total dislocation density which can be tracked back to glissile junctions on the same level.

Detailed investigations have been carried out to characterize the blocking nature dislocation junctions and their relation to hardening [7–9], in general assuming all junctions to be sessile [10]. This study focuses on the dislocation multiplication aspect of glissile junctions as a follow up to Ref. [6] with a more detailed study on the role of the crystallographic orientation with respect to tensile loading direction, on the influence of the sample size and internal length scale of the dislocation microstructure.

The starting point is an assumption about the size and dislocation density regime, where the glissile junction acts as a source mechanism. The working hypothesis is, that this mechanism occurs and contributes to the plastic deformation if the probability of junction formation in a sample is high (activation of multiple glide systems) and the plastic deformation is junction controlled as opposed to single source controlled plasticity [11–13]. This leads to two parameters: The first one being $d\sqrt{\rho}$, where d is the smallest outer dimension of the sample and ρ the total dislocation density, connecting an internally developed length scale with an external one [14]. The second one is the crystallographic orientation in tensile direction: in a multi-slip orientation, more glide systems have a higher Schmid factor, resulting in their respective activation under loading and therefore to a higher probability of junctions, as opposed to a single-slip orientation.

This work explores the regime, where the glissile junction is a possible source by varying sample size and dislocation density. Additionally we also address the question if the earlier found correlation of stress drops in the global stress strain curves with the formation of glissile junctions [6] is an alternative explanation to

* Corresponding author.
E-mail addresses: markus.stricker@kit.edu (M. Stricker), daniel.weygand@kit.edu (D. Weygand).
[1] Principal corresponding author.

http://dx.doi.org/10.1016/j.actamat.2015.07.073
1359-6454/

the relation of strain bursts with avalanche like depinning events [15,16].

2. The glissile junction

The formation of a dislocation junction involves two dislocations characterized by $(\mathbf{b}_I, \mathbf{n}_I)$, where $\mathbf{b}_I$ and $\mathbf{n}_I$ are the Burgers vector and glide plane normal of the Ith dislocation. In case of a glissile junction, lets assume that the Burgers vector of dislocation 1 ($\mathbf{b}_1$) is parallel to the intersection line of the two involved glide planes. For an orientation of the two dislocations which leads to an attractive elastic interaction, the junction formed is glissile on the second glide plane [4,17] for purely geometrical reasons and characterized by $(\mathbf{b}_1 + \mathbf{b}_2, \mathbf{n}_2)$. From all possible junctions in the fcc crystal, the glissile junction is geometrically the most frequent with 48 out of possible 132 junctions. The result of the junction is a mobile dislocation on the new glide system $(\mathbf{b}_3, \mathbf{n}_2)$, which is populated by this mechanism (Fig. 1). The junction – or better the new dislocation – is therefore a Frank–Read (FR) source with endpoints that are free to slide along the intersection line of both glide planes. Therefore under applied load the length and thus the critical source strength depends on the loading on all three glide systems involved in the glissile junctions. In the following, this newly formed dislocation is called glissile to indicate its origin.

Another mechanism producing dislocation density on a new glide system is cross-slip. In this case the glide plane normal changes, while the Burgers vector is constant.

3. Method/setup

Discrete dislocation dynamics (DDD) codes are nowadays commonly used to simulate plastic deformation of small samples by tracking the motion of dislocations [18–22]. In the code used, dislocations are discretized as piecewise linear segments [17,20,23]. Their motion is computed based on the externally applied load and the elastic interaction between dislocations. Physical mechanisms like junctions and cross-slip are included.

In order to address the role of the initial dislocation structure [24] on the observed mechanism, different schemes to generate an initial dislocation microstructure are realized. There are numerous ways too choose an initial configuration, ranging from randomly distributed FR sources with variable activation stress, prismatic loops, relaxed structures or cutting out the initial configuration for simulations from a much larger bulk specimen [25] with subsequent relaxation.

In the present work, three types of initial structures are used:

(i) Initial structures consisting of randomly distributed FR sources (w.r.t. position, orientation in plane and length). These are distributed randomly in the sample, but a homogeneous population of all glide planes is ensured. The length of the sources is $2\,\rho_{\mathrm{ini}}^{-1/2} \pm 20\%$, where ρ_{ini} is the initial dislocation density. This value is chosen to be in a multiplication controlled regime [26].
(ii) Initial structures resulting from a relaxation calculation of a structure consisting of randomly distributed closed loops (radius, center) on different glide systems. These loops can be much larger than the simulation volume itself and only pierce through it with a small piece of the arc or lie completely inside the volume. All 12 glide systems of the fcc crystal are populated with the same number of loops prior to relaxation. During relaxation a dislocation network without artificial pinning points is formed [24].
(iii) This initial structure is basically the same as (ii) but skipping the relaxation process. It is methodically close to cutting out a part of a bulk simulation and using this as an initial structure [25] with the accompanying amount of microplasticity at very small strains.

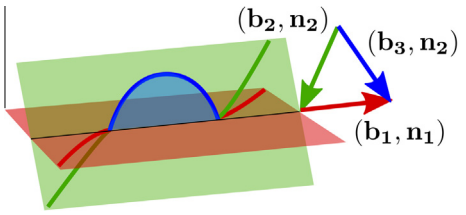

Fig. 1. The glissile junction: glide system $(\mathbf{b}_1, \mathbf{n}_1)$, red, where $\mathbf{b}_1$ is parallel to the intersection line, reacts with glide system $(\mathbf{b}_2, \mathbf{n}_2)$, green, to form a new glide system $(\mathbf{b}_3, \mathbf{n}_2)$, blue. (For interpretation of the references to colour in this figure caption, the reader is referred to the web version of this article.)

All micropillars have an aspect ratio of 3 and a square cross-section of side length d with the long axis along the tensile direction to reduce the influence of the displacement controlled boundaries at the top and bottom [27]. The chosen side lengths d are 0.5, 1.0, 1.5 and 2.0 μm.

The samples are subjected to uniaxial tensile loading, where at the bottom layer, the components of all displacements are set to zero and at the top layer a strain rate of $\dot{\varepsilon} = 5000\,\mathrm{s}^{-1}$ in tensile direction is prescribed, while leaving the in plane components traction free. On all other boundaries zero tractions are prescribed and thus dislocations are allowed to leave the volume. To study the role of the crystallographic orientation, the tensile axes have been varied from single-slip to multislip orientations: $\langle 100\rangle, \langle 110\rangle, \langle 111\rangle, \langle 234\rangle$.

Depending on the orientation, the 12 slip systems of the fcc crystal have different Schmid factors, which allows to evaluate the role of differently activated glide system on junction formation and multiplication. The distribution of the 12 Schmid factors are: $\langle 100\rangle$-orientation: 8 glide systems have the same Schmid factor, while all others are zero, $\langle 111\rangle$ has 6 non-zero, $\langle 110\rangle$ has 4 non-zero and the $\langle 234\rangle$-orientation has one dominant while the others are non-zero but small. In order to be able to distinguish the origin of a dislocation, a tracking scheme has been implemented to identify dislocations, which are newly generated by glissile junctions. The marked dislocations may themselves participate in the formation of junctions. In case of a glissile junction, this would lead to a next generation (generation 2 and higher) of dislocations marked as glissile. Furthermore it is possible to discriminate between those glissile dislocations initially present prior to the loading and those generated during further loading. This is needed for samples with an initial dislocation network generated by relaxation (initial condition (ii)), already containing many glissile junctions. With this it is possible to account only for those which are newly generated during straining in the further analysis.

This marker is then used in a post-processing step to compute the contribution of dislocations marked as *glissile* to the total dislocation density and plastic deformation. In this counting scheme, all further interactions (e.g. cross-slip) of this dislocation are included, because if the mechanism would not exist, all subsequent events would not have happened in this exact same way.

The plastic strain is evaluated via the formula

$$\varepsilon_{ij}^{\mathrm{pl}} = \sum_{I=1}^{N} \frac{A_I}{2V} \left(b_{I,i} n_{I,j} + b_{I,j} n_{I,i} \right), \tag{1}$$

where N is the number of dislocations in the sample, A_I is the swept area, V the total volume of the sample, $b_{I,i}$ the components of the Burgers vector and $n_{I,i}$ the components of the glide plane normal

vector of dislocation I. Depending on the marker, the contribution of individual dislocations is added to the plastic strain of glissile or all other dislocations.

4. Results

Fig. 2 shows the dislocation network of a sample with side length $d = 1\,\mu m$ from a directly strained configuration at $\varepsilon_{tot} = 0.5\%$ (initial condition (iii)). The straining direction is along $\langle 1\,1\,0\rangle$ and the coloring is according to the glide plane normal for those dislocations which can be tracked back to a glissile junction. All other dislocations are shown in black. The figure shows visually that a substantial fraction of dislocation density is the result of glissile junctions, suggesting that the deformation behavior is greatly influenced by this source mechanism.

To work out the occurrence of the glissile junction and its role in plastic deformation with respect to orientation and sample size, 250 samples have been simulated. Table 1 gives an overview of the data base for the evaluation. The number of configurations per size is chosen according to the outer dimension: The smaller the outer dimension, the more samples were simulated, since smaller samples are subjected to a higher statistical variation [13,27,28]. All reported samples are loaded to a total strain of $\varepsilon_{tot} = 0.5\%$ and all values of $d\sqrt{\rho}$ are measured at this point. In order to illustrate the role of the initial dislocation structure one example for each type is presented. Fig. 3 shows a data set from a sample with an initial microstructure consisting of FR sources only (case (i)), comprising the overall stress–strain curve, the evolution of the total dislocation density, a junction count for Lomer, glissile, collinear and Hirth junction as well as cross-slip. Additionally, the fraction of dislocation density from glissile dislocations f_G and the plastic strain vs. the total strain are depicted. The stress–strain curve shows a linear elastic regime along with a slight increase in dislocation density due to the bowing out of dislocations. When the stress reaches the critical stress needed to activate existing FR sources, the sample starts deforming plastically. With the onset of plasticity, junctions form and the glissile junction is the second most common junction at $\varepsilon_{tot} = 0.5\%$. The fraction of glissile dislocation density f_G rises and their glide motion contributes about 30% to the plastic deformation in tensile direction for this particular sample.

Fig. 4 shows a data set from a sample initialized with closed loops, which was relaxed prior to loading (case (ii)). The linear elastic regime in the stress–strain curve is less pronounced, which is also reflected in the density evolution: during the first 0.05% of total strain approximately 20% of the dislocations leave the volume. This is due to the loss of unstable parts of the dislocation network which are formed during relaxation and leads to a nonlinear increase in stress during straining (microplasticity). The junction count of this initial structure is in essence quite similar to the one initialized with FR sources with cross-slip and the glissile junction being the most common junction. Also the trend for the fraction of dislocation density from glissile dislocations f_G and the contribution to the plastic deformation in tensile direction is on the same order (approx. 50%).

Fig. 5 shows a data set from a sample initialized with closed loops, which was directly strained (case (iii)). Additionally to the pronounced microplasticity at the beginning of the loading, the total dislocation density decreases to approximately one third of the initial value and then stays almost constant during further straining. This is due to the initial relaxation process, where unstable parts of the dislocation network are eliminated. The glissile junction is the most common junction and f_G at $\varepsilon_{tot} = 0.5\%$ is on the order of 75% associated with a contribution to plastic deformation in tensile direction of approx. 60%.

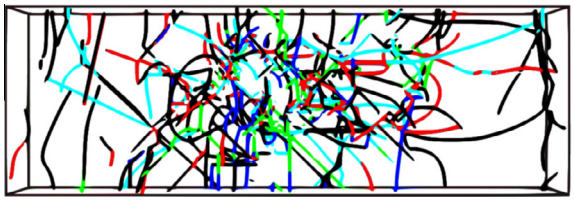

Fig. 2. Visualization of a dislocation network at $\varepsilon_{tot} = 0.5\%$: sample size $d = 1.0\,\mu m$, tensile straining direction $\langle 1\,1\,0\rangle$. Dislocations are colored according to their glide plane normal if they are a product of a glissile junction. All other dislocations are colored in black.

Table 1
Overview of simulated number of realizations sorted by size d with corresponding $d\sqrt{\rho}$ values at 0.5% total strain. The number of configurations is the sum over all initial configurations (i)–(iii) and crystallographic orientations per size.

Size d [μm]	# configs per size	$d\sqrt{\rho}$ range at $\varepsilon_{tot} = 0.5\%$
0.5	99	0.8–7.3
1.0	100	0.2–10.3
1.5	40	0.6–8.4
2.0	11	2.1–9.9

Fig. 6 shows a compilation of the fraction of glissile dislocation density f_G at the reference deformation of $\varepsilon_{tot} = 0.5\%$ from all simulations. The data points are split up into subfigure for each tensile axis, going from single slip (lower subfigure) to multislip (upper subfigure). For values of $d\sqrt{\rho}$ larger than 4, for the $\langle 1\,0\,0\rangle$ and $\langle 1\,1\,1\rangle$, more than $f_G \geqslant 0.1$ can be tracked back to glissile junctions. For the $\langle 1\,1\,0\rangle$ and $\langle 2\,3\,4\rangle$ direction there are no precise points where f_G is always larger than 0.1. But the majority of simulations show a value of $f_G \geqslant 0.1$.

Fig. 7 shows the corresponding fraction of the plastic strain in tensile direction attributed to glissile junctions from all simulations at $\varepsilon_{tot} = 0.5\%$. Again, the data points are split into subfigures for each tensile axis with an increase of active slip systems from the lower to the upper subfigures. A tendency is apparent: When moving from the lower left to the upper right corner in either the single directions or globally in the figure, glissile dislocations contribute more to the plastic strain.

Based on the observation that changes in f_G, the glissile junction count and the plastic strain contribution of glissile dislocations are often connected with stress-drops, a correlation analysis is performed. Fig. 8 shows the connection between the individual data series: During the massive stress-drop occurring between 0.25% and 0.3% total strain, the glissile junction counter increases sharply, the density fraction f_G shows a rapid change and the additional plastic strain, which causes the relaxation in stress, is largely attributed to the glide of glissile dislocations within the sample.

Consequently, a statistical analysis of all stress drops in the data base is performed. For this the stress rate, plastic strain from glissile junctions and the total plastic strain are evaluated in post processing (based on Eq. (1)). But this procedure it is not exactly the same as the calculation of the plastic strain during the simulation, where the plastic strain contribution is evaluated based on the displacement fields of the dislocations. Hence the data from post-processing is sorted according to the agreement to the plastic strain calculated from the stress–strain evolution which is given by

$$\varepsilon_{pl} = \varepsilon_{tot} - \frac{\sigma}{E}, \tag{2}$$

where E is the Young's modulus (cf. Appendix A for a detailed explanation of the sorting). The total plastic strain is inversely linear correlated with the stress, yielding a correlation Pearson coefficient of $r = -1$.

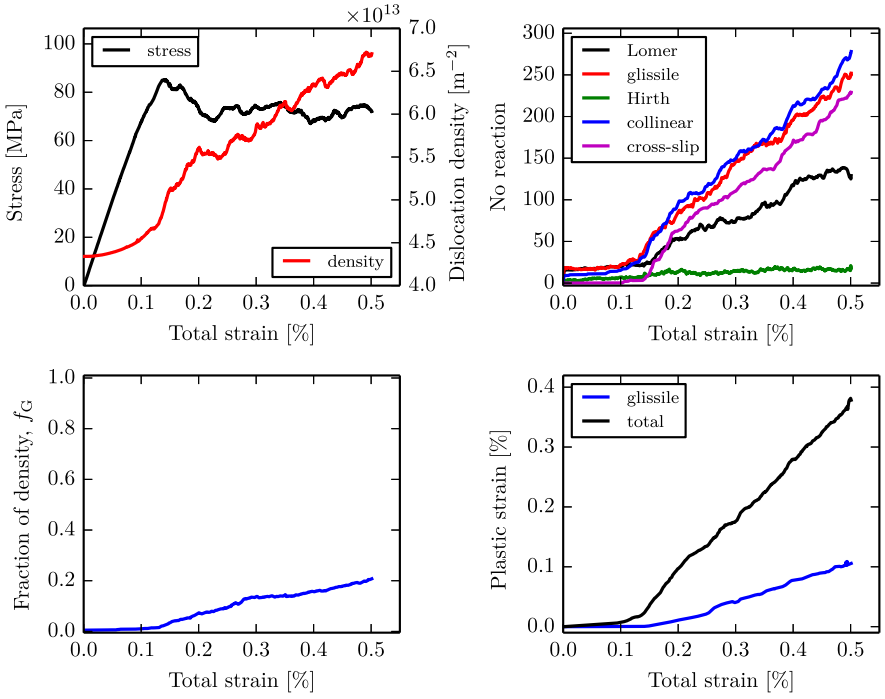

Fig. 3. Data set of a sample with $d = 1.0$ μm initialized with FR sources and strained in ⟨100⟩ direction: Stress–strain behavior, total dislocation density evolution, junction count, evolution of f_G and the plastic strain over total strain as well as the contribution from glissile dislocations. The final state is characterized by $d\sqrt{\rho} = 8.19$.

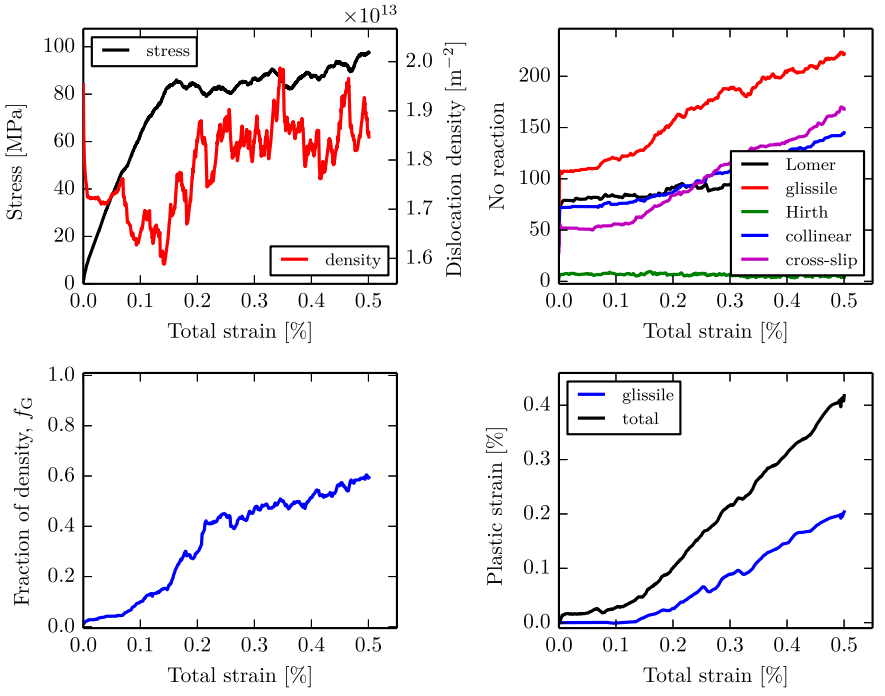

Fig. 4. Data set of a sample with $d = 1.0$ μm. The initial structure is the result of a relaxation process (case (ii)) and then strained in ⟨100⟩ direction: Stress–strain behavior, total dislocation density evolution, junction count, evolution of f_G and the plastic strain over total strain as well as the contribution from glissile dislocations. The final state is characterized by $d\sqrt{\rho} = 4.3$.

After sorting, 28 out of 46 (60%) of the considered stress drops show a higher correlation for the plastic strain resulting from the motion of glissile dislocations than from all other dislocations. The mean correlations for glissile plastic strain and other plastic strain are $r_{gl} = -0.75$ and $r_{oth} = -0.12$ respectively.

5. Discussion

The results from the 250 simulations show that glissile junctions form in the studied size and density regime. Depending on the crystallographic orientation of the tensile loading axis and a

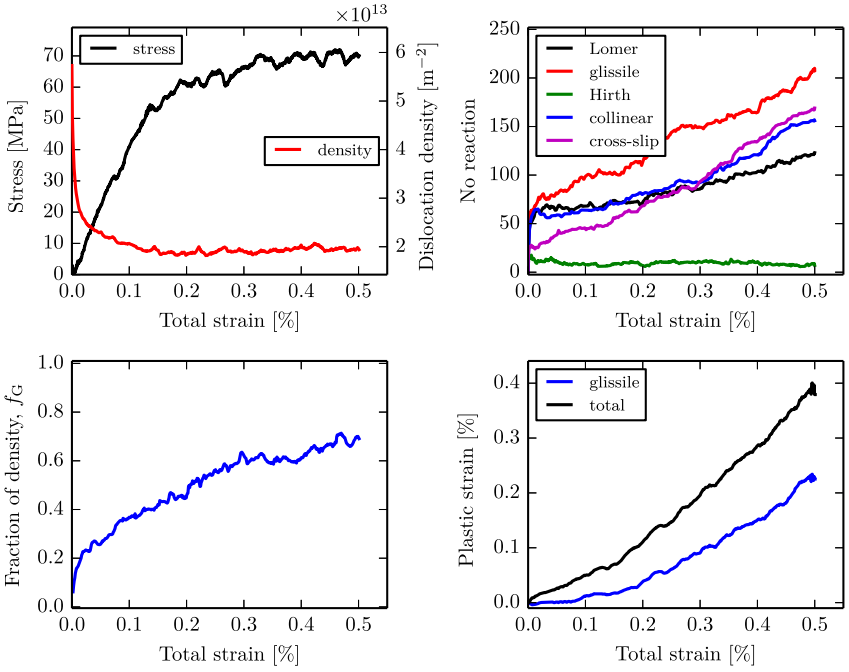

Fig. 5. Data set of a 1.0 μm sample. It is initialized with randomly distributed closed loops then directly strained (case (iii)) in ⟨100⟩ direction: Stress–strain behavior, total dislocation density evolution, junction count, evolution of f_G and the plastic strain over total strain as well as the contribution from glissile dislocations. The final state is characterized by $d\sqrt{\rho} = 4.4$.

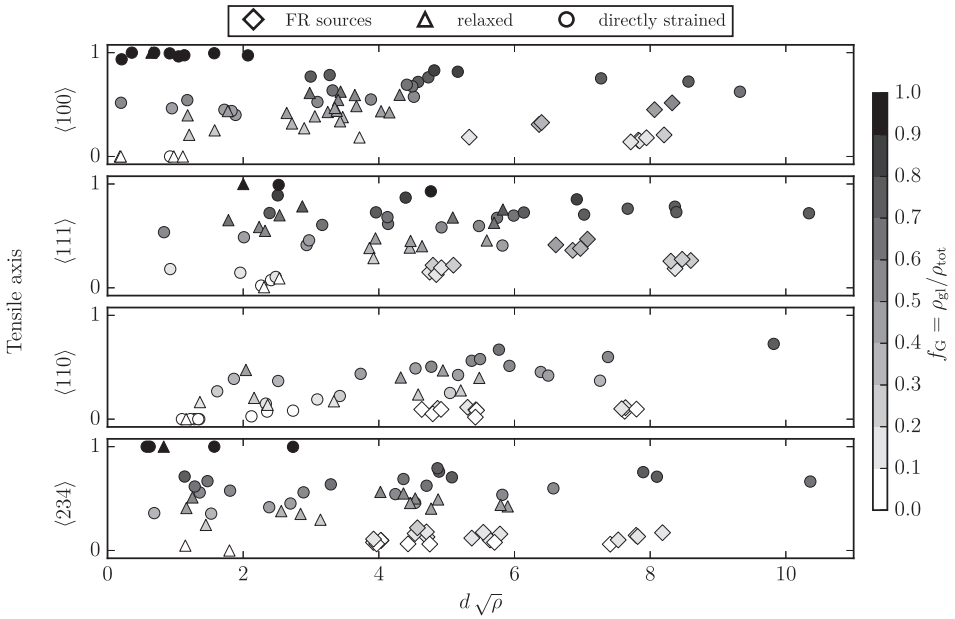

Fig. 6. Fraction f_G of total density resulting from glissile junctions at reference point $\varepsilon_{tot} = 0.5\%$, for each tensile axis. The symbols shown on top indicate the respective scheme used for generating the initial configuration of each data point.

dimensionless parameter $d\sqrt{\rho}$, the total dislocation density consists up to over 90% of glissile dislocations (cf. Fig. 6). The comparison of the density fraction f_G of glissile dislocations (Fig. 6) to the contribution to plastic deformation in tensile direction (Fig. 7) suggests the following correlation: the glissile source does not only produce dislocations on a new slip system, but these dislocations glide and contribute to the plastic deformation on the order of their density fraction f_G. Fig. 7 also shows clearly, that a strong scatter exists in the values for a given $d\sqrt{\rho}$. In small scale samples, statistical scatter is commonly observed and is a signature of the answer of a particular initial dislocation microstructure [12,28]. For the smallest sample dimension ($d = 0.5$ μm, Fig. 9) a strong statistical variation for the lower values of $d\sqrt{\rho}$ is observed. Due to the small number of dislocations and the unfavorable surface to volume ratio limiting dislocation multiplication, the system answers are often binary (cf. also Fig. 11): For similar and small values of $d\sqrt{\rho}$, the fraction of plastic strain resulting from the motion of glissile dislocations is either almost 0 or 1. The weakest source relaxes the system by multiple activation and therefore the contribution to the plastic strain is given by the type of the weakest source: (a) preexisting source or (b) a new source generated by a glissile junctions leading to a $f_G \approx 1$.

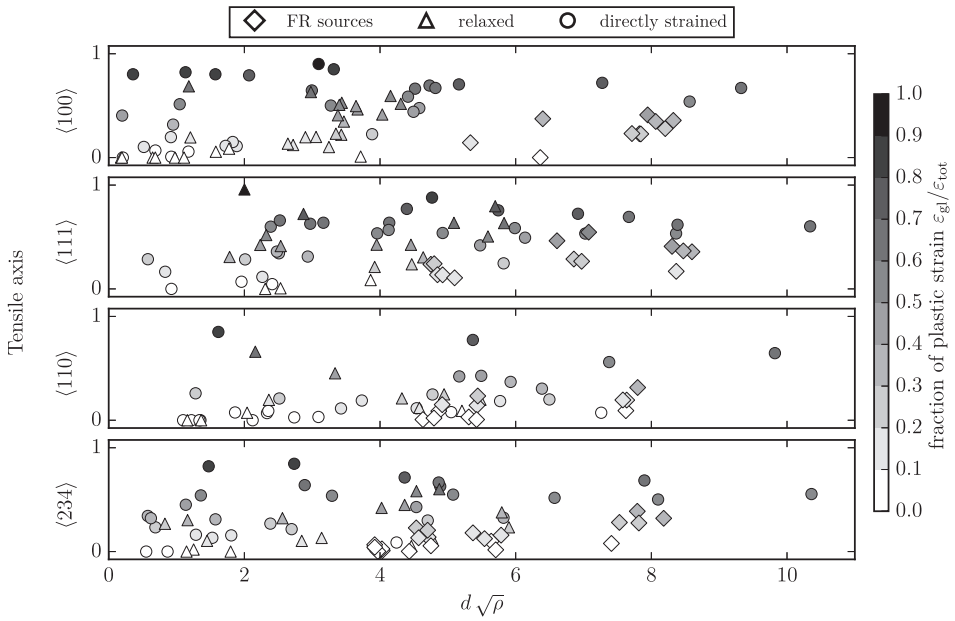

Fig. 7. Fraction of plastic strain from glissile dislocations at $\varepsilon_{tot} = 0.5\%$. For the legend description, refer to Fig. 6. The symbols shown on top indicate the respective scheme used for generating the initial configuration of each data point.

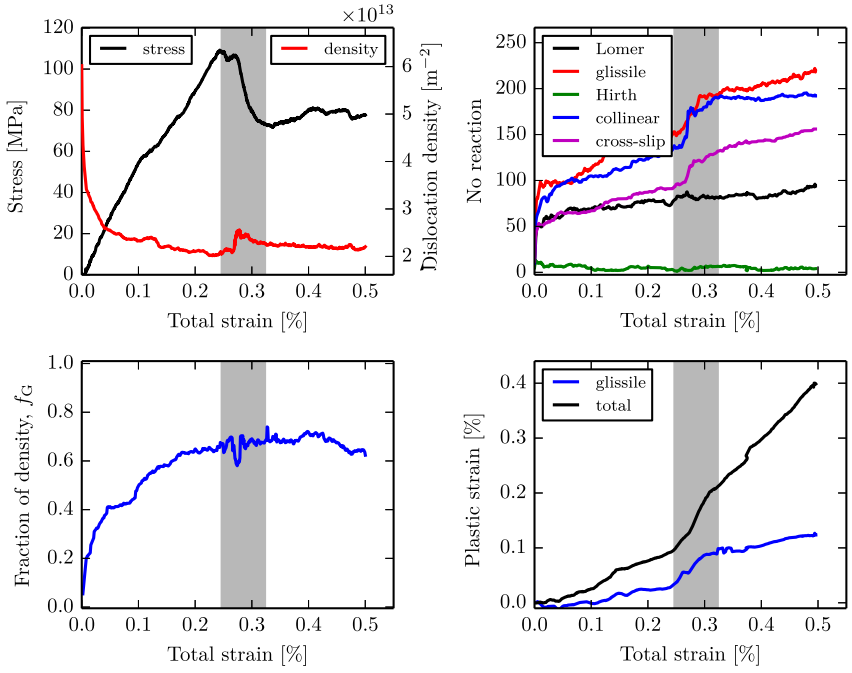

Fig. 8. Data set of a sample with $d = 1.0$ µm, directly strained in ⟨2 3 4⟩ direction: Stress–strain behavior, total dislocation density evolution, junction count, evolution of f_G and the plastic strain over total strain as well as the contribution from glissile dislocations. The end state is characterized by $d\sqrt{\rho} = 4.69$. Additionally the stress drop is marked in gray.

With increasing initial $d\sqrt{\rho_{ini}}$, the single source operation becomes less dominant and the probability for dislocation junctions inside the volume rises, leading to storage of dislocations and therefore also higher value $d\sqrt{\rho}$ at a total strain of 0.5%. For values $d\sqrt{\rho}$ larger than about 4 the scatter of the plastic slip contribution from glissile dislocations decreases. This can be explained with a higher probability for dislocations to meet and form junctions, based on the larger volume for the dislocation network to develop and a higher density. The observed trend continues with the two larger sample sizes or increasing $d\sqrt{\rho}$ (cf. Fig. 10).

It is therefore concluded that around the value of $d\sqrt{\rho} \approx 4$ the different system sizes and densities behave similar. The plasticity is then increasingly controlled by collective behavior leading to new junctions and subsequent dislocation multiplication, due to the activation of glissile junctions.

Another point to be addressed is the role of the initial microstructure on the observed multiplication mechanism by glissile junctions. The main difference in the behavior of the different initial structures is observed in the elastic regime: While the relaxed (ii) and directly strained (iii) samples exhibit strong

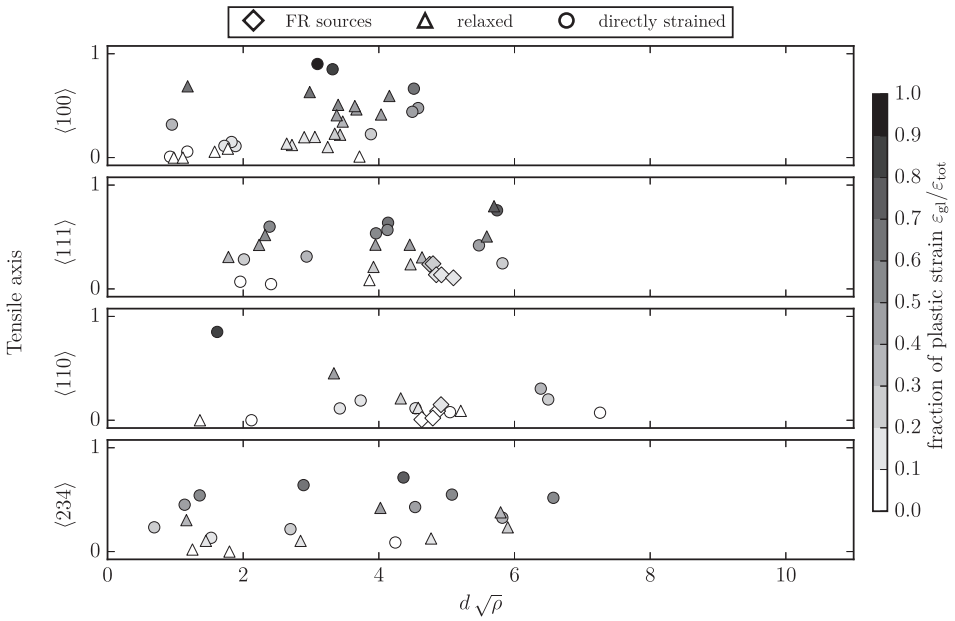

Fig. 9. Fraction of plastic strain resulting from glissile junctions for sample size $d = 0.5$ μm at the reference point. For legend refer to Fig. 6.

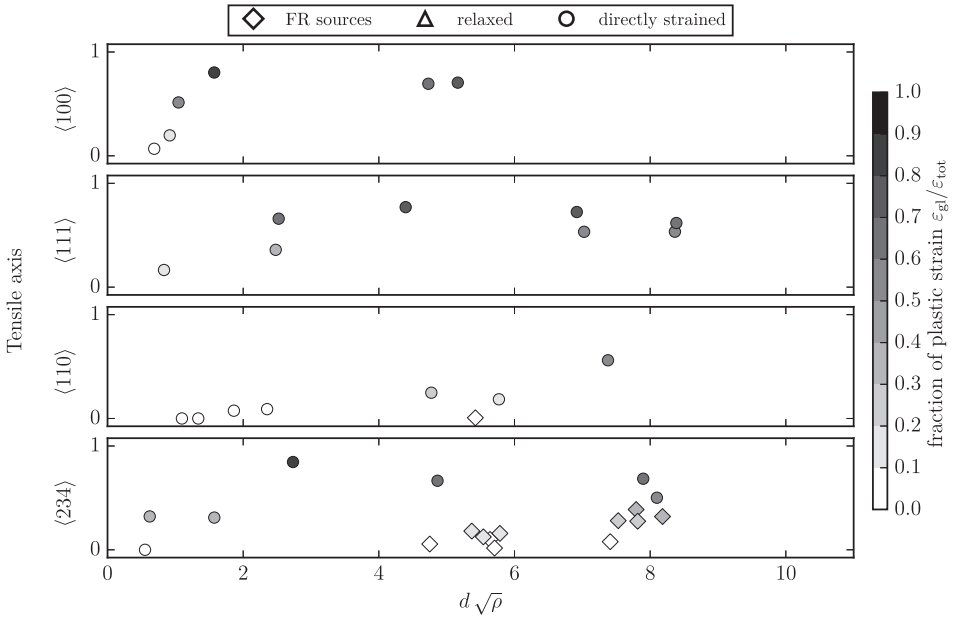

Fig. 10. Fraction of plastic strain resulting from glissile junctions for sample size $d = 1.5$ μm at the reference point. For legend refer to Fig. 6.

microplastic behavior due to the elimination of weak parts of the initial dislocation network, the FR sources (i) only bow out upon an increase of stress, lowering the effective elastic modulus. All three types of initial configurations show the same trends with respect to the importance of glissile junctions as a dislocation source and plastic slip at a total strain of 0.5%. The trend is even more pronounced in pinning point free initial structures, which are considered to be more realistic since no artificial constraint is imposed on the dislocation microstructure. This can be rationalized as follows: in a structure based on initial FR sources, these can only be blocked but not destroyed by glide processes and dislocation interactions. Therefore preexisting FR sources are activated more easily, due to their persistent nature, and contribute more to the overall plastic slip. The first type of initial configuration (i) has been included since it is a known way of initializing DDD samples [27–31].

In order to investigate the role of the crystallographic orientation on the dislocation multiplication process due to glissile junctions, the contribution of plastic strain from glissile dislocations is plotted in Fig. 11 for the four crystallographic orientation studied. Furthermore an averaged value for $\varepsilon_{gl}/\varepsilon_{tot}$ with a binning width of 1 for $d\sqrt{\rho}$ dependency is plotted including the respective standard deviations. Additionally, a linear least square fit, assuming a linear relation, is shown. From this linear fit an increase of the fraction $\varepsilon_{gl}/\varepsilon_{tot}$ for the considered range within $d\sqrt{\rho}$ (=1 to 10) is observed. For the multislip orientations ⟨100⟩ and ⟨111⟩ one could also argue for a saturation of the ratio $\varepsilon_{gl}/\varepsilon_{tot}$, which might be due to the limited amount of data available for those

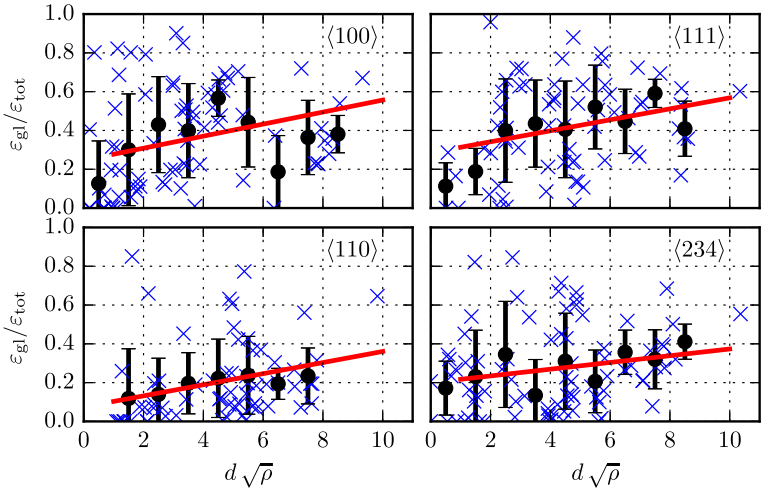

Fig. 11. Contribution of plastic strain versus $d\sqrt{\rho}$ from glissile junctions, individual simulations as crosses, binned mean values with standard deviations and a linear least square fit for all four directions.

values. Assuming the validity of the linear least square fits for all directions, the Fig. 12 can be plotted. The figure allows for two conclusions: (1) the three multislip orientations ($\langle 100\rangle, \langle 111\rangle, \langle 110\rangle$) have almost the same slope; (2) the multislip orientations show a higher slope than single slip orientation ($\langle 234\rangle$). This can be rationalized by statistical arguments on the probability of junction formation: in case of multislip, many dislocation glide systems are activated and the probability to form junctions – a junction formation rate – between the systems is high. Furthermore the probability that those junctions lead to glissile sources with a high Schmid factor is high. Taking the $\langle 100\rangle$ crystallographic orientation, 8 slip systems with equal non-zero Schmid factor exist, while the remaining slip system have a Schmid factor of 0. Therefore the generated glissile dislocation is either on a glide system with the highest Schmid factor or zero [6]. In case of single slip the situation is different: dislocations on the glide system with the highest Schmid factor glide through an essentially immobile dislocation forest, leading to a number of stable glissile junctions, which have therefore a low Schmid factor. Accordingly, a lower formation rate for dislocations due to glissile junctions is expected. A second scenario is also possible in single slip: due to dislocation glide on low Schmid factor planes a glissile junction can be formed, which acts as dislocation source on the glide system with the high Schmid factor. The corresponding production rate is low compared to the multi-slip condition. Therefore for both formation processes of glissile junctions a lower rate is found, reflected in the lower slope shown in Fig. 12. The difference in absolute values of y-axis interceptions is attributed to the limited amount of data sets. These differences might level out with increasing number of considered simulations having an equal distribution of $d\sqrt{\rho}$ values.

In order to address the geometrical extension of the formed glissile junctions, the average distance between the endpoints of the junction – called junction length – is determined. From this length the critical stress to activate the newly formed Frank–Read source can be estimated. Fig. 13 shows the average junction length per simulation of glissile junctions over the smallest sample dimension d for all simulations (crosses) at $\varepsilon_{tot} = 0.5\%$, the mean values with standard deviation and a linear fit: with increasing sample dimension d, the maximum junction length increases. This trend confirms that weaker sources of glissile origin can form with increasing sample dimension. The formation of weaker sources depending on sample size was already observed with FR-initialized samples, but the contribution to the plastic strain was not evaluated [28].

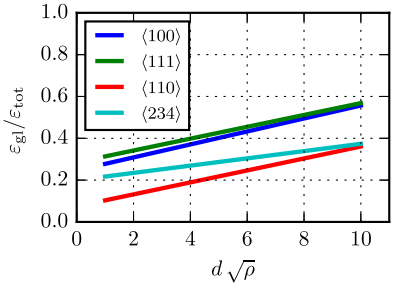

Fig. 12. Comparison of all linear least square fits for the contribution of plastic deformation from glissile junctions.

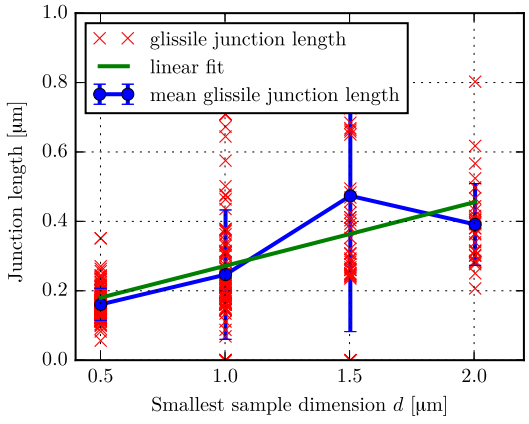

Fig. 13. Glissile junction length at 0.5% total strain as a function of smallest sample dimension for all simulations. Crosses mark averages from individual simulations, blue the mean values per size with standard deviation and the simple line represents a linear fit.

The analysis of stress drops in displacement controlled deformation setups shows that these can be related to the formation of glissile junctions. The calculation of the Pearson correlation coefficient based on data sets from stress drops, shows a direct connection of the motion of glissile dislocations with stress drops. In more than half of the regarded stress drops, the correlation between the plastic strain from glissile dislocations is higher than the one from all other dislocations. This hints to a not yet understood connection between the glissile junction and sudden changes in stress.

All the arguments above lend itself for an incorporation in a continuum plasticity model. And while dislocation junctions are already being included in continuum models in the context of hardening, the observed dislocation source mechanism based on glissile junctions is currently not included in existing crystal plasticity formulations [3,8,32] or higher order continuum dislocation density theories [33–35]. To include this mechanism, a dislocation density based formulation can be extended as follows: The nomenclature of Fig. 1 for the two interacting systems $1,2$ and the glissile system 3 is used. The glissile junction produces new dislocation density on a system 3, which is different from the two reacting dislocations. A rate formulation for the increase of density on the glide system (ρ_3) is chosen. Following the argumentation of [8], the junction formation rate between an active system and a forest system is calculated. Here we consider that system 1 and 2 can play either role, active or forest system. The junction formation rate of a dislocation density in encountering a forest density is derived via a collision frequency. The average dislocation spacing of one slip system is given by

$$L_J \propto \frac{1}{\sqrt{\rho_J}} \tag{3}$$

where $J = 1,2$ for each slip system forming a possible glissile junction on system 3. The collision frequencies v_I for both slip systems is the given by

$$v_I = \frac{v_I}{L_J} \quad J \neq I \tag{4}$$

where v_I are the respective velocities of the dislocation on slip system I. The total production rate of density on the glissile system $\dot{\rho}_3$ is due to junction formation of mobile dislocations on system 1 with system 2 or vice versa and reads

$$\dot{\rho}_3 \propto \rho_1 v_1 + \rho_2 v_2. \tag{5}$$

Using the Orowan equation $\dot{\gamma}_I = \rho_I b\, v_I$ for each system I leads to

$$\dot{\rho}_3 = c_1\sqrt{\rho_2}\|\dot{\gamma}_1\| + c_2\sqrt{\rho_1}\|\dot{\gamma}_2\|, \tag{6}$$

where c_I are constants, which depend on the Burgers vector modulus b and the effective junction length generated by the individual junction process. As the interaction rate is sign independent, the absolute values of the slip rates are used. The proposed equation for $\dot{\rho}_3$ shows a physically reasonable limiting behavior: in order to have a non zero contribution, both dislocation densities ρ_I must be non-zero and additionally at least one density has to be mobile to form junctions, ensured by the respective $\dot{\gamma}_I$. In case of multislip, a higher production rate is expected from Eq. (6) in agreement with the DDD results. The constants c_I have to be determined and this will be addressed in future work. Furthermore an annihilation rate of $-\dot{\rho}_3$ for the dislocation density on the systems 1 and 2 has to be included, to take into account the loss of the corresponding dislocation density on the reacting systems.

6. Conclusion

An new dislocation multiplication mechanism based on glissile junctions has been characterized with respect to its overall contribution to the plastic slip and dislocation density. This work extends the initial observation of the mechanism for a $\langle 100\rangle$ multislip tensile loading [6]. The current work clearly shows that the formation of glissile junctions is a common event. The density produced by this mechanism is mobile and contributes to the plastic deformation within the considered size and density regime. Depending on density, sample size and crystallographic orientation, the glissile junction is responsible for the major part of the density and plastic deformation. Starting from a value of around $d\sqrt{\rho} \approx 4$, the system responses are more homogeneous due to the collective behavior of the dislocation ensemble. Then plasticity is governed by dislocation junctions and multiplication as opposed to single source plasticity for smaller values of $d\sqrt{\rho}$. Furthermore similar to the earlier observation on the formation of weaker sources through dislocation junctions [28], weaker glissile sources are generated for larger samples.

A correlation between stress drops and the formation of glissile junctions is found and the Pearson correlation coefficient r between stress drops and plastic strain from glissile junctions is higher in ≈60% of the cases, but it is unclear if this is just a transition regime, where the specimen is relaxed on an initially dislocation-free glide system or an observation which still holds for larger strains. Within this regime, the glissile junction provides an alternative view to avalanche like depinning effects [15].

Even though the observations in DDD are made on small scale specimens and a direct transfer to bulk behavior is not obvious, an extrapolation to bulk is motivated from this observation: For a high value of $d\sqrt{\rho}$, the system responses are less scattered, indicating a more stable state. Therefore the incorporation of glissile junctions as a source mechanism in continuum models such as crystal plasticity and higher order dislocation continuum theories is worthwhile. A possible functional form for a dislocation density production term suited for crystal plasticity models is proposed. An implementation of the additional term and extension to different crystallographies is planned in a future work.

Acknowledgements

The financial support for the research group FOR1650 *Dislocation based plasticity* funded by the German Research Foundation (DFG) under contract number WE3544/5-1 is gratefully acknowledged. This work was performed on the computational resource bwUniCluster funded by the Ministry of Science, Research and Arts and the Universities of the State of Baden-Württemberg, Germany, within the framework program bwHPC, on the IC2 (funded by the DFG) and the HC3 at the Steinbuch Centre for Computing at Karlsruhe Institute of Technology.

Appendix A. Correlation sorting

Calculating the plastic strain in two different ways leads to slight variations with respect to time, and its derivative (rate) amplifies these little changes, destroying a linear relationship between the stress and plastic strain. Therefore the data is sorted according to the following rules in the given order:

(1) All data, where the stress rate is positive (stress increase) is neglected, since only stress drops are of interest. Individual drops are regarded as *whole* data sets for the correlation analysis regardless of their size.
(2) The Pearson correlation coefficient r is calculated for each stress drop between the stress rate and the total plastic strain rate from post processing. All data sets with an $r > -0.8$ are neglected, based on the assumption that e.g. the alignment of the data sets from post processing and during simulation with respect to total strain is not correct.
(3) From the remaining stress drops, the correlation coefficients are calculated for each stress drop:
  (a) Pearson correlation between stress rate and plastic strain rate from glissile junctions.
  (b) Pearson correlation between stress rate and the plastic strain rate from all other dislocations.

References

[1] P. Franciosi, M. Berveiller, A. Zaoui, Latent hardening in copper and aluminium single crystals, Acta Metall. 28 (1980) 273–283.
[2] F. Nabarro, F. Nabarro, J. Hirth, Dislocations in solids, Dislocations In Solids, vol. 12, North-Holland Publ, 2004.
[3] L. Kubin, B. Devincre, T. Hoc, Modeling dislocation storage rates and mean free paths in face-centered cubic crystals, Acta Mater. 56 (2008) 6040–6049.
[4] G. Saada, P. Veyssiere, Work hardening of face centred cubic crystals, Dislocation intersection and cross-slip, in: Dislocations in Solids, vol. 11, 2002, p. 413.
[5] D. Hull, D.J. Bacon, Introduction to Dislocations, vol. 37, Elsevier, 2011.
[6] D. Weygand, Mechanics and dislocation structures at the micro-scale: insights on dislocation multiplication mechanisms from discrete dislocation dynamics simulations, in: Dislocation Plasticity, MRS Proceedings, vol. 1651, 2014.
[7] R. Madec, B. Devincre, L. Kubin, T. Hoc, D. Rodney, The role of collinear interaction in dislocation-induced hardening, Science 301 (2003) 1879–1882.
[8] A. Ma, F. Roters, A constitutive model for fcc single crystals based on dislocation densities and its application to uniaxial compression of aluminium single crystals, Acta Mater. 52 (2004) 3603–3612.
[9] V.V. Bulatov, L.L. Hsiung, M. Tang, A. Arsenlis, M.C. Bartelt, W. Cai, J.N. Florando, M. Hiratani, M. Rhee, G. Hommes, et al., Dislocation multi-junctions and strain hardening, Nature 440 (2006) 1174–1178.
[10] B. Devincre, L. Kubin, T. Hoc, Physical analyses of crystal plasticity by DD simulations, Scr. Mater. 54 (2006) 741–746.
[11] T.A. Parthasarathy, S.I. Rao, D.M. Dimiduk, M.D. Uchic, D.R. Trinkle, Contribution to size effect of yield strength from the stochastics of dislocation source lengths in finite samples, Scr. Mater. 56 (2007) 313–316.
[12] S. Rao, D. Dimiduk, T. Parthasarathy, M. Uchic, M. Tang, C. Woodward, Athermal mechanisms of size-dependent crystal flow gleaned from three-dimensional discrete dislocation simulations, Acta Mater. 56 (2008) 3245–3259.
[13] O. Kraft, P.A. Gruber, R. Mönig, D. Weygand, Plasticity in confined dimensions, Annu. Rev. Mater. Res. 40 (2010) 293–317.
[14] M. Zaiser, S. Sandfeld, Scaling properties of dislocation simulations in the similitude regime, Model. Simul. Mater. Sci. Eng. 22 (2014) 065012.
[15] F.F. Csikor, C. Motz, D. Weygand, M. Zaiser, S. Zapperi, Dislocation avalanches, strain bursts, and the problem of plastic forming at the micrometer scale, Science 318 (2007) 251–254.
[16] B. Devincre, T. Hoc, L. Kubin, Dislocation mean free paths and strain hardening of crystals, Science 320 (2008) 1745–1748.
[17] D. Weygand, P. Gumbsch, Study of dislocation reactions and rearrangements under different loading conditions, Mater. Sci. Eng. A 400–401 (2005) 158–161.
[18] L.P. Kubin, G. Canova, M. Condat, B. Devincre, V. Pontikis, Y. Bréchet, Dislocation microstructures and plastic flow: a 3D simulation, Solid State Phenom. 23 (1992) 455–472.
[19] M. Fivel, M. Verdier, G. Canova, 3D simulation of a nanoindentation test at a mesoscopic scale, Mater. Sci. Eng. A 234–236 (1997) 923–926.
[20] D. Weygand, L.H. Friedman, E.V. der Giessen, A. Needleman, Aspects of boundary-value problem solutions with three-dimensional dislocation dynamics, Model. Simul. Mater. Sci. Eng. 10 (2002) 437–468.
[21] W. Cai, A. Arsenlis, C.R. Weinberger, V.V. Bulatov, A non-singular continuum theory of dislocations, J. Mech. Phys. Solids 54 (2006) 561–587.
[22] G. Po, N. Ghoniem, A variational formulation of constrained dislocation dynamics coupled with heat and vacancy diffusion, J. Mech. Phys. Solids 66 (2014) 103–116.
[23] D. Weygand, J. Senger, C. Motz, W. Augustin, V. Heuveline, P. Gumbsch, High performance computing and discrete dislocation dynamics: plasticity of micrometer sized specimens, in: W.E. Nagel, D.B. Kröner, M.M. Resch (Eds.), High Performance Computing in Science and Engineering '08, Springer, Berlin, Heidelberg, 2009, pp. 507–523.
[24] C. Motz, D. Weygand, J. Senger, P. Gumbsch, Initial dislocation structures in 3-d discrete dislocation dynamics and their influence on microscale plasticity, Acta Mater. 57 (2009) 1744–1754.
[25] C. Zhou, S.B. Biner, R. LeSar, Discrete dislocation dynamics simulations of plasticity at small scales, Acta Mater. 58 (2010) 1565–1577.
[26] X. Zhang, K.E. Aifantis, J. Senger, D. Weygand, M. Zaiser, Internal length scale and grain boundary yield strength in gradient models of polycrystal plasticity: how do they relate to the dislocation microstructure?, J Mater. Res. 29 (2014) 2116–2128.
[27] J. Senger, D. Weygand, C. Motz, P. Gumbsch, O. Kraft, Aspect ratio and stochastic effects in the plasticity of uniformly loaded micrometer-sized specimens, Acta Mater. 59 (2011) 2937–2947.
[28] J. Senger, D. Weygand, P. Gumbsch, O. Kraft, Discrete dislocation simulations of the plasticity of micro-pillars under uniaxial loading, Scr. Mater. 58 (2008) 587–590.
[29] V. Bulatov, W. Cai, Computer Simulations of Dislocations, Oxford Series on Materials Modelling Series, OUP Oxford, 2006.
[30] A. Arsenlis, W. Cai, M. Tang, M. Rhee, T. Oppelstrup, G. Hommes, T.G. Pierce, V.V. Bulatov, Enabling strain hardening simulations with dislocation dynamics, Model. Simul. Mater. Sci. Eng. 15 (2007) 553.
[31] B. Devincre, L.P. Kubin, Simulations of forest interactions and strain hardening in fcc crystals, Model. Simul. Mater. Sci. Eng. 2 (1994) 559.
[32] F. Roters, P. Eisenlohr, L. Hantcherli, D. Tjahjanto, T. Bieler, D. Raabe, Overview of constitutive laws, kinematics, homogenization and multiscale methods in crystal plasticity finite-element modeling: theory, experiments, applications, Acta Mater. 58 (2010) 1152–1211.
[33] T. Hochrainer, M. Zaiser, P. Gumbsch, A three-dimensional continuum theory of dislocation systems: kinematics and mean-field formulation, Philos. Mag. 87 (2007) 1261–1282.
[34] K. Schulz, D. Dickel, S. Schmitt, S. Sandfeld, D. Weygand, P. Gumbsch, Analysis of dislocation pile-ups using a dislocation-based continuum theory, Model. Simul. Mater. Sci. Eng. 22 (2014) 025008.
[35] T. Hochrainer, S. Sandfeld, M. Zaiser, P. Gumbsch, Continuum dislocation dynamics: towards a physical theory of crystal plasticity, J. Mech. Phys. Solids 63 (2014) 167–178.